3854 *Chem. Mater.* **2010,** *22,* 3854–3861
DOI:10.1021/cm903583f

CHEMISTRY OF MATERIALS
Article

Preparation of Crystallized Mesoporous Ta_3N_5 Assisted by Chemical Vapor Deposition of Tetramethyl Orthosilicate

Takashi Hisatomi,[†] Michiko Otani,[†,‡] Kiyotaka Nakajima,[§,⊥] Kentaro Teramura,[†,||] Yoko Kako,[†] Daling Lu,[‡,§] Tsuyoshi Takata,[†] Junko N. Kondo,[§] and Kazunari Domen*[,†,‡]

[†]*Department of Chemical System Engineering, School of Engineering, The University of Tokyo,* [‡]*Research Office of Solution-Oriented Research for Science and Technology (SORST), and* [§]*Chemical Resources Laboratory, Tokyo Institute of Technology.* [⊥]*Current Affiliation: Materials and Structures Laboratory, Tokyo Institute of Technology.* [||]*Current Affiliation: Pioneering Research Unit for Next Generation, Kyoto University.*

Received November 26, 2009. Revised Manuscript Received May 26, 2010

Ordered mesoporous Ta_3N_5 with crystalline thin-wall structures was successfully obtained from an amorphous mesoporous Ta_2O_5 by nitridation at 1073 K under flowing NH_3 (500 mL min^{-1}). The silica layer that was deposited on the pore wall by chemical vapor deposition of tetramethyl orthosilicate and later easily removed by alkaline treatment was indispensible for preserving the original mesostructure against phase transition during crystallization and nitridation. Mesoporous Ta_3N_5 has a mesoporosity and mesoporous structure similar to that of amorphous Ta_2O_5 and crystallized pore walls composed of orthorhombic Ta_3N_5. The BET surface area, pore size, and wall thickness of mesoporous Ta_3N_5 were approximately 100 m^2 g^{-1}, 4 nm, and 2 nm, respectively. Mesoporous Ta_3N_5 loaded with Pt nanoparticles was active for photocatalytic H_2 evolution from an aqueous methanol solution under visible light ($\lambda > 420$ nm). The photocatalytic activity of mesoporous Ta_3N_5 was three times that of conventional bulk Ta_3N_5 under the same reaction conditions because of the former's thin crystallized pore wall (ca. 2 nm in thickness), which enabled efficient charge transfer of photoexcited electrons and holes to surface active sites.

1. Introduction

Mesoporous transition metal oxides, prepared by a sol−gel reaction of network-forming metal precursors in the presence of surfactant molecules as structure-directing agents,[1,2] have attracted much attention because of their potential applications in catalysts,[3−5] photocatalysts,[6−11] and electronic[12] and magnetic devices.[13] In catalytic applications, the mesoporosity of transition metal oxides can greatly enhance the access of reactant molecules to the catalytic active sites on their internal surface, resulting in higher catalytic activities as compared to the corresponding bulk catalysts.[14] The thin-wall structure derived from the periodic mesoporous structure offers an additional advantage for photocatalytic application by significantly shortening the migration length of photoexcited carriers to surface active sites. Representative examples are mesoporous Ta_2O_5[6] and $MgTa_2O_6$,[7] which despite their amorphous structure exhibit higher photocatalytic activity for water splitting into H_2 and O_2 than the corresponding nonporous crystallized oxides. The inorganic phase in mesoporous transition metal oxides usually remains amorphous because the amorphous-to-crystalline phase transformation is accompanied by the destruction of the original mesoporous structure. Because the mobility of photoexcited carriers is generally limited in an amorphous structure, photoexcited electrons and holes readily recombine before contributing to the desired photocatalytic reactions, negating the advantages of mesoporosity in photocatalysis.[15] Thus, the development of a general strategy for the preparation of crystallized

*Corresponding author. Address: Department of Chemical System Engineering, School of Engineering, The University of Tokyo, 7-3-1 Hongo, Bunkyo-ku, Tokyo 113-8656, Japan. Tel:+81-3-5841-1148. Fax:+81-3-5841-8838. E-mail: domen@chemsys.t.u-tokyo.ac.jp.

(1) Yang, P.; Zhao, D.; Margolose, D. I.; Chmelka, B. F.; Stucky, G. D. *Nature* **1998**, *396*, 152–155.
(2) Yang, P.; Zhao, D.; Margolose, D. I.; Chmelka, B. F.; Stucky, G. D. *Chem. Mater.* **1999**, *11*, 2813–2826.
(3) Wong, M. S.; Huang, H. C.; Ying, J. Y. *Chem. Mater.* **2002**, *14*, 1961–1973.
(4) Hiyoshi, M.; Lee, B.; Lu, D.; Hara, M.; Kondo, J. N.; Domen, K. *Catal. Lett.* **2004**, *98*, 181–186.
(5) Goettmann, F.; Le Floch, P.; Sanchez, C. *Chem. Commun.* **2006**, 180–182.
(6) Takahara, Y.; Kondo, J. N.; Takata, T.; Lu, D.; Domen, K. *Chem. Mater.* **2001**, *13*, 1194–1199.
(7) Kondo, J. N.; Uchida, M.; Nakajima, K.; Lu, D.; Hara, M.; Domen, K. *Chem. Mater.* **2004**, *16*, 4304–4310.
(8) Sakatani, Y.; Grosso, D.; Nicole, L.; Biossiére, C.; Soler-Illia, G. J.; de, A. A.; Sanchez, C. *J. Mater. Chem.* **2006**, *16*, 77–82.
(9) Noda, Y.; Lee, B; Domen, K; Kondo, J. N. *Chem. Mater.* **2008**, *20*, 5361–5367.
(10) Inumaru, K.; Kasahara, T.; Yasui, M.; Yamanaka, S. *Chem. Commun.* **2005**, 2131–2133.
(11) Kuwahara, Y.; Maki, K.; Matsumura, Y.; Kamegawa, T.; Mori, K.; Yamashita, H. *J. Phys. Chem. C* **2009**, *113*, 1552–1559.
(12) Jiao, F.; Bruce, P. G. *Adv. Mater.* **2007**, *19*, 657–660.
(13) Jiao, F.; Jumas, J.-C; Womes, M.; Chadwick, A. V.; Harrison, A.; Bruce, P. G. *J. Am. Chem. Soc.* **2006**, *128*, 12905–12909.
(14) Sayari, A. *Chem. Mater.* **1996**, *8*, 1840–1852.
(15) Kondo, J. N.; Domen, K. *Chem. Mater.* **2008**, *20*, 835–847.

 Published on Web 06/08/2010

transition metal oxides with an ordered mesoporous structure is keenly awaited.

Recently, we have developed a synthetic method for the preparation of a crystallized mesoporous transition metal oxide, based on reinforcing the mesoporous structure with a thermally resistant organic[16] or inorganic "scaffold".[17] For instance, silica backfilling method using a silicone compound, bis(trimethylsiloxy)methylsilane, as a mesopore filler, has been found to be effective in stabilizing the ordered mesoporous structure against crystallization,[17] yielding the desired crystallized materials that retain their original mesoporous structure after crystallization. Silicone reagents, reacting with surface OH groups to form Si−O−M (M: metal cation) bonds, are transformed into amorphous silica by thermal decomposition. Because the amorphous silica accumulating in the mesopores of amorphous Ta_2O_5 functions as a "scaffold" that hinders mass transfer upon phase transition, amorphous Ta_2O_5 is successfully crystallized, with the mesoporosity and mesoscopic ordering retained. As expected, crystallized mesoporous Ta_2O_5 exhibits a much higher activity for overall water splitting than nonporous crystalline and mesoporous amorphous Ta_2O_5, because of the efficient transfer of photoexcited carriers to surface active sites through the thin-wall crystalline phase.[9]

Despite such high photocatalytic performance, these mesoporous transition metal oxides are active only under UV light irradiation because their bandgap energies are too large to absorb visible light ($\lambda > 400$ nm).[6,7,9] Because UV light constitutes only a few percent of the photons in the solar spectrum, a mesoporous photocatalyst material active under visible light is strongly desired in order to develop high-performance photocatalytic systems. Our group has reported that oxynitrides and nitrides containing pentavalent Ta ions, such as TaON,[18,19] Ta_3N_5,[18] and $BaTaO_2N$,[20] are potentially effective for photocatalytic water splitting under visible light. The band gap energies of these materials are considerably lower than those of the corresponding oxide semiconductors. For example, the band gap energies of Ta_2O_5, TaON, and Ta_3N_5 are estimated to be 3.9, 2.4, and 2.1 eV, respectively.[21] Ta_3N_5 shows photocatalytic activity for photoreduction and photooxidation of water under visible light irradiation up to approximately 600 nm in the presence of sacrificial electron donors and acceptors, respectively.[18] This means that the band structure of Ta_3N_5 is suitable for photocatalytic water splitting under visible light irradiation, although overall water splitting has not yet been accomplished on Ta_3N_5 presumably because of immediate recombination of photoexcited carriers before reaching catalytically active sites on the surface. This background prompted us to develop a crystallized mesoporous Ta_3N_5, which would significantly improve photocatalytic activity because of the advantages of its crystallized thin-wall structure.

In this study, we applied a "silica scaffold method" based on chemical vapor deposition (CVD) of a volatile silicone precursor (tetramethyl orthosilicate; TMOS) as an effective strategy to fortify the mesopore wall of Ta_2O_5 prior to nitridation at high temperature. The silica-coated mesoporous Ta_2O_5 thus obtained was used as a starting material for the preparation of mesoporous Ta_3N_5. The TMOS-CVD treatment has two purposes: First, the silica layer deposited homogeneously on the pore wall of the mesoporous Ta_2O_5 serves as a scaffold against phase transition during nitridation of the mesoporous oxide. Second, the CVD treatment enables us to tune the thickness of the silica layer and thus prevent complete filling of the mesopores.[22] As a result, the nitrogen source can continue to reach the Ta_2O_5 inside the mesopores even after introduction of the "silica scaffold" by CVD. It is therefore expected that the TMOS-CVD method will prove preferable to the conventional silica backfilling method for the development of mesoporous Ta_3N_5. Finally, photocatalytic activity of the crystallized mesoporous Ta_3N_5 was evaluated by H_2 evolution from an aqueous methanol solution under visible light irradiation ($\lambda > 420$ nm).

2. Experimental Section

2.1. Preparation of Crystallized Mesoporous Ta_3N_5. A hexagonal mesoporous Ta_2O_5 prepared by a previously reported procedure was used as an amorphous precursor.[23] Briefly, 1 g of triblock copolymer P-123 was dissolved in 10 g of ethanol with constant stirring for 60 min. To this solution was added 6 mmol of $TaCl_5$ with vigorous stirring for 10 min, followed by the addition of 6 mmol of deionized water with stirring for more than 1 h to promote hydrolysis. The resulting sol solution was transferred to Petri dishes for aging at 313 K for 7 days to obtain a gel precursor. The gel was then calcined at 773 K for 5 h to remove the template, yielding amorphous mesoporous Ta_2O_5.

The amorphous precursor was modified with a silica layer by the TMOS-CVD treatment after evacuation pretreatment at 523 K. The cycle of TMOS-CVD treatment consisted of five exposures of the sample to TMOS vapor for 1 min at 473 K with evacuation in each interval and two subsequent exposures to water vapor in the same manner. The TMOS molecules adsorbed on the sample were hydrolyzed by the water supply to form hydroxyl groups. A portion of the hydroxyl groups were dehydrated to form the silica layer, while some remaining hydroxyl groups reacted with the TMOS supplied in the next cycle. The optimum conditions for the TMOS-CVD treatment depend on the amount of surface hydroxyl groups on the material. In the case of mesoporous Ta_2O_5, the TMOS-CVD

(16) Katou, T.; Lee, B.; Lu, D.; Kondo, J. N.; Hara, M.; Domen, K. *Angew. Chem., Int. Ed.* **2003**, *42*, 2382–2385.
(17) Shirokura, N.; Nakajima, K.; Nakabayashi, A.; Lu, D.; Hara, M.; Domen, K.; Tatsumi, T.; Kondo, J. N. *Chem. Commun.* **2006**, 2188–2190.
(18) Hara, M.; Hitoki, G.; Takata, T.; Kondo, J. N.; Kobayashi, H.; Domen, K. *Catal. Today* **2003**, *78*, 555–560.
(19) Higashi, M.; Abe, R.; Ishikawa, A.; Takata, T.; Ohtani, B.; Domen, K. *Chem. Lett.* **2008**, *37*, 138–139.
(20) Higashi, M.; Abe, R.; Takata, T.; Domen, K. *Chem. Mater.* **2009**, *21*, 1543–1549.
(21) Chun, W.-J.; Ishikawa, A.; Fujisawa, H.; Takata, T.; Kondo, J. N.; Hara, M.; Kawai, M.; Matsumoto, Y; Domen, K. *J. Phys. Chem. B* **2003**, *107*, 1798–1803.
(22) Ishimaru, R.; Shibasaki, Y.; Hara, M.; Ueda, M.; Domen, K.; Kondo, J. N. *Chem. Lett.* **2005**, *34*, 596–597.
(23) Nakajima, K.; Hara, M.; Domen, K; Kondo, J. N. *Chem. Lett.* **2005**, *34*, 394–395.

treatment cycle was repeated five times, in view of the hydrophobicity of mesoporous Ta_2O_5.[24] A typical molar ratio of Si to Ta for silica-coated sample was estimated to be 0.2 by inductive coupled plasma optical emission spectroscopy (ICP−OES). The amorphous mesoporous Ta_2O_5 coated with silica was used as precursor for mesoporous Ta_3N_5. The precursor was placed in a tube furnace and heated under a flow of 500 mL min^{-1} of NH_3 at 773−1123 K for 0.5−30 h. After the nitridation, the silica layers were removed by treating the nitrided samples with alkaline solution (pH 14) at room temperature for 4 h. The final products were collected by filtration and drying under ambient conditions. For comparison, bulk Ta_3N_5 was prepared by nitriding commercially available Ta_2O_5 powder at 1123 K for 15 h under a flow of 500 mL min^{-1} of NH_3.[18]

2.2. Characterization. Powder X-ray diffraction (XRD) patterns of the products were obtained on a Philips X'Pert-MPD PW3500 diffractometer or Rigaku RINT-UltimaIII Bragg−Brentano type X-ray diffractometer with Cu Ka radiation (40 kV, 40 mA) at a scan rate of 1.0 deg min^{-1} over the range $0.3° < 2\theta < 60.0°$. Diffuse reflection spectra were obtained using a Jasco V−560 UV−visible diffuse reflectance spectrometer. Nitrogen adsorption−desorption isotherms were measured at 77 K using a Beckman Coulter SA-3100 system or BEL Japan BELSORP-mini. Prior to measurement, the samples were pretreated at 423 K for more than 1 h under a vacuum. BET surface areas were estimated over a relative pressure (p/p_0) range of 0.05 to 0.30. Pore size distributions were obtained by analyzing the adsorption branch of the isotherms using the BJH method. TG-DTA analyses were performed using a Shimadzu DTG-50 in air at a heating rate of 10 K min^{-1}. TEM images were captured using a JEOL 2010F electron microscope operated at 200 keV. The ratios of Si to Ta in the products before and after alkali treatment were analyzed by ICP-OES using a Thermo Elemental Iris Advantage DuO.

2.3. Photocatalytic H_2 Evolution Reaction Using Crystallized Mesoporous Ta_3N_5. To assess the photocatalytic performance of the Ta_3N_5 samples, photocatalytic H_2 evolution reaction from an aqueous methanol solution was performed in a top-irradiation Pyrex reaction vessel connected to a closed gas circulation and evacuation system. The Ta_3N_5 sample (0.20 g) nitrided at 1073 K for 7 h was suspended in 200 mL of an aqueous, 80 vol % methanol solution containing an appropriate amount of H_2PtCl_6. After the system was degassed completely, the reaction solution was irradiated by a 300-W Xe lamp equipped with a cutoff filter ($\lambda > 420$ nm). During the irradiation, Pt particles were deposited on the Ta_3N_5 at a rate of 0.05 or 3 wt % with respect to the Ta_3N_5 as a result of the reduction of $[PtCl_6]^{4-}$ by photoexcited electrons, and served as reduction sites for H^+ in the production of gaseous H_2.[25] In this reaction, photoexcited holes immediately oxidizes methanol to formaldehyde, formic acid, and eventually CO_2 instead of water,[26] which suppresses recombination of photoexcited carriers, and backward reactions involving CO_2 are negligible because of the small change in Gibbs free energy (+ 9 kJ mol^{-1}). Photocatalytic H_2 evolution is promoted in the presence of methanol as a sacrificial reagent. Therefore, this reaction is not overall water splitting, but a test reaction to examine the potential ability of a semiconductor that does not show perceivable activity in overall water splitting reaction. The evolved gases were analyzed by a gas chromatograph (GC-8A, TCD, Ar carrier, MS5A column). Bulk Ta_3N_5 and standard TiO_2 powder (P-25, Degussa) were used as reference catalysts for comparison.

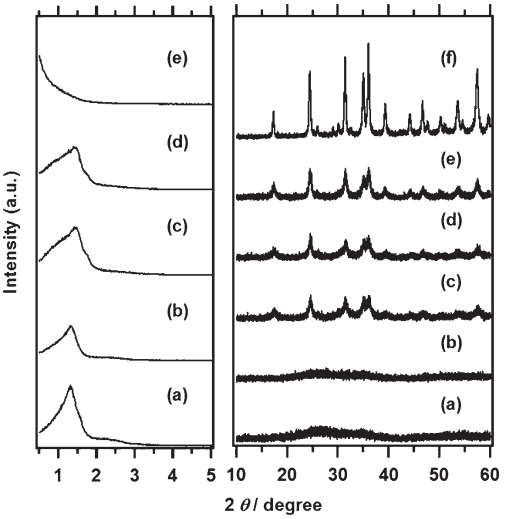

Figure 1. XRD patterns for (a) the amorphous precursor, (b) the silica-coated mesoporous Ta_2O_5, (c) the silica-coated mesoporous Ta_3N_5 after nitridation, (d) the mesoporous Ta_3N_5 after alkaline treatment, and (e) the nitrided sample without TMOS-CVD treatment. (f) Bulk Ta_3N_5 for reference. Nitridation temperature, 1073 K; nitridation time, 7 h; alkaline treatment temperature, room temperature; alkaline treatment time, 4 h.

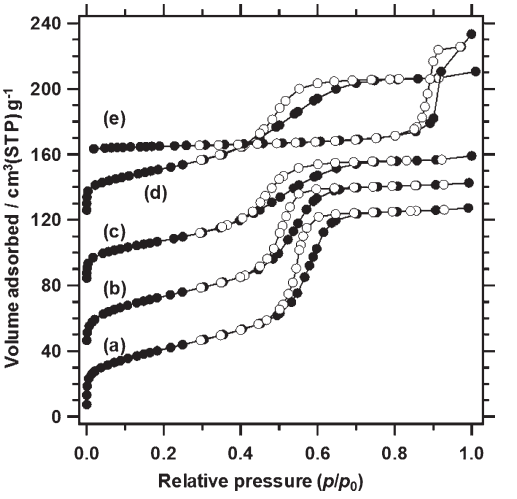

Figure 2. N_2 adsorption−desorption isotherms for (a) the amorphous precursor, (b) the silica-coated mesoporous Ta_2O_5, (c) the silica-coated mesoporous Ta_3N_5 after nitridation, and (d) the mesoporous Ta_3N_5 after alkaline treatment, and (e) the sample nitrided without silica layer. Nitridation temperature, 1073 K; nitridation time, 7 h; alkaline treatment temperature, room temperature; alkaline treatment time, 4 h. The isotherms are shifted by 40 $cm^3(STP)\ g^{-1}$, respectively.

3. Results and Discussion

3.1. Preparation of Crystallized Mesoporous Ta_3N_5 Assisted by the TMOS-CVD Method. The XRD patterns, N_2 adsorption−desorption isotherms, pore size distribution curves, and physical properties of the mesoporous Ta_2O_5 before and after nitridation at 1073 K for 7 h are shown in Figures 1 and 2 and Figure S1 in the Supporting Information, respectively, as well as Table 1. The BET surface area and pore volume of conventional Ta_3N_5 prepared from commercial Ta_2O_5 powder are also listed

(24) Kondo, J. N.; Lu, D.; Takahara, Y.; Maruya, K.; Domen, K; Tatsumi, T. *Bull. Chem. Soc. Jpn.* **2000**, *73*, 1123–1129.
(25) Kraeutler, B.; Bard, A. J. *J. Am. Chem. Soc.* **1978**, *100*, 4317–4318.
(26) Kawai, T.; Sakata, T. *J. Chem. Soc., Chem. Commun.* **1980**, 694–695.

Table 1. Physical Properties of Mesoporous Ta_2O_5

	S_{BET} ($m^2\ g^{-1}$)	pore volume ($cm^3\ g^{-1}$)	pore size (nm)	wall thickness (nm)
(a) amorphous precursor	146	0.20	4.8	3.0
(b) silica-coated mesoporous Ta_3O_5	123	0.17	4.2	3.2
(c) (b) after nitridation	101	0.12	3.7	3.3
(d) (c) after alkaline treatment	114	0.14	3.7	3.4
(e) directly nitrided mesoporous Ta_2O_5	18	0.11	24	
conventional Ta_3N_5[a]	12	0.04		

[a] Prepared from commercial Ta_2O_5 by nitridation at 1123 K for 15 h.

in Table 1 for comparison. The small-angle XRD profile in Figure 1a reveals that the amorphous Ta_2O_5 precursor had a typical ordered mesostructure, characterized by an intense diffraction peak at $2\theta = 1.31°$ with an additional peak at 2.27°. The isotherm of the amorphous Ta_2O_5 precursor (Figure 2a) was a typical type-IV pattern with a clear H1-type hysteresis loop, which has been shown to be characteristic of materials with a cylindrical pore geometry and a highly uniform pore size (see Figure S1a in the Supporting Information). The BET surface area, mesopore volume, and pore size of the amorphous Ta_2O_5 precursor were estimated to be 146 $m^2\ g^{-1}$, 0.20 $cm^3\ g^{-1}$, and 4.8 nm, respectively. After direct nitridation of the nontreated amorphous Ta_2O_5 precursor, the isotherm changed from a type-IV to type-III pattern (Figure 2e), as is characteristic of a nonporous oxide. The resulting nitride had a BET surface area of 18 $m^2\ g^{-1}$ and a mesopore volume of 0.11 $cm^3\ g^{-1}$, both lower than those for the amorphous precursor. Moreover, the diffraction peak arising from mesoscopic ordering of the original Ta_2O_5 was entirely absent in the XRD pattern (Figure 1e). This result is quite similar to our previous study on crystallization of mesoporous Ta_2O_5[9] and indicates that the phase transition from amorphous Ta_2O_5 to crystallized Ta_3N_5 without silica reinforcement was generally accompanied by collapse of the original mesostructure. Note that relatively large pore volume of this sample (0.11 $cm^3\ g^{-1}$) resulted from the interparticle voids between Ta_3N_5 nanoparticles.

The XRD profile, N_2 adsorption−desorption isotherm, and pore size distribution curve for the silica-coated mesoporous Ta_2O_5 were quite similar to those of the amorphous Ta_2O_5 precursor (Figures 1b and 2b, and Figure S1b in the Supporting Information). The silica-coated Ta_2O_5 had a BET surface area of 123 $m^2\ g^{-1}$ and a mesopore volume of 0.17 $cm^3\ g^{-1}$. The reduced pore size and the narrow pore size distribution curve of the silica-coated Ta_2O_5 (see Figure S1b in the Supporting Information) suggest that silica was deposited homogeneously on the internal and external surfaces of the amorphous Ta_2O_5 by TMOS-CVD treatment. The changes in pore size from 4.8 to 4.2 nm and in wall thickness from 3.0 to 3.2 nm are not necessarily attributable to the introduction of the silica layer because condensation of the amorphous Ta_2O_5 framework was promoted by the hydration−dehydration treatments in the TMOS-CVD method. Thus, the thickness of the silica layer on the pore wall cannot be simply estimated from the difference in pore size or wall thickness between the amorphous precursor and the silica-coated Ta_2O_5.

The XRD patterns for the silica-coated mesoporous Ta_2O_5 after nitridation (Figure 1c) and after alkaline treatment (Figure 1d) showed intense signals in the small-angle region and several peaks in the wide-angle region, which were assignable to the mesoporous structure and orthorhombic Ta_3N_5, respectively. This indicated that nitridation of Ta_2O_5 took place successfully even in the presence of the silica layer, and that the amorphous pore wall of the silica-coated Ta_2O_5 was successfully nitrided without significant degradation of the original mesoporous structure. The diffraction peaks for orthorhombic Ta_3N_5 were significantly weaker and broader than those observed for conventional Ta_3N_5. This suggests that the silica layer on the pore wall hindered rearrangement of the constituent elements and large-scale crystal growth. In fact, the diffraction peak intensities were not increased by severer nitridation, as described in section 3.2. The isotherms of the resulting Ta_3N_5 samples were type-IV patterns with H1-type hysteresis loops (Figure 2c) similar to that of the amorphous Ta_2O_5 precursor. The decreases in BET surface area (101 $m^2\ g^{-1}$), mesopore volume (0.12 $cm^3\ g^{-1}$), and pore size (3.7 nm) that occurred during the phase transition from amorphous Ta_2O_5 to orthorhombic Ta_3N_5 were associated with the increase in the density of the mesopore framework, because substitution of 3 O^{2-} anions by 2 N^{3-} anions inevitably caused the original mesoporous structure to shrink. The broadening of the pore size distribution curve for mesoporous Ta_3N_5 (see Figure S1c in the Supporting Information) was due to the partial degradation of original mesoporous structure and mesoporosity during the nitridation. The alkaline treatment could remove more than 80% of the silica deposited on the surface, which resulted in recovery of both the surface area (114 $m^2\ g^{-1}$) and the pore volume (0.14 $cm^3\ g^{-1}$).

The mesoporous and crystalline structure of the obtained sample was confirmed by TEM observation of pores and lattice fringes. The TEM image of the mesoporous Ta_3N_5 (Figure 3) revealed the presence of ordered mesopores (white lines) clearly while mesoporous structure were slightly distorted as compared with amorphous Ta_2O_5 precursor. These results are in good agreement with those of XRD and N_2 adsorption−desorption analysis and indicate that the silica layer prevents large-scale crystal growth of Ta_3N_5, which accompanies the severe destruction of mesoporous structure. The lattice fringes extended coherently across several mesopore channels. Thus, the crystalline mesoporous Ta_3N_5 prepared through the TMOS-CVD method was not a mixture of an

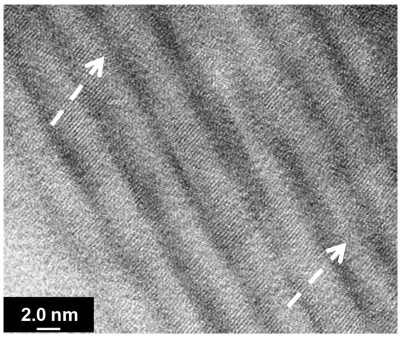

Figure 3. TEM image of mesoporous Ta_3N_5. As indicated by the arrows, the lattice fringes extend coherently across several mesopores.

ordered amorphous mesoporous material and a nonporous crystalline material, but a mesoporous material with crystallized pore wall. The crystallite size of Ta_3N_5 in the mesoporous structure can be estimated from the Scherrer's equation.[27] Given that Scherrer constant was 0.9, the crystallite size was estimated to be 9 nm with the (110) diffraction peak at $2\theta = 24.6°$. The crystallite size was thus larger than the thickness of mesopore wall and not simply limited by the thickness of mesopore wall. Similar results were obtained in our previous studies on crystallized mesoporous oxides,[9,15−17] One possible explanation for the development of larger Ta_3N_5 crystallites than the thickness of the mesopore wall is formation of planar-like Ta_3N_5 crystallites: if thin and planar crystallites grow up in mesopore walls with a honeycomb-like structure, the crystallite sizes can be larger than the wall thickness and the lattice fringes could appear across the mesopores as shown in Figure 3. Although crystallization mechanism and crystalline structure of the mesoporous Ta_3N_5 are under investigation, it is reasonable to conclude that the direct nitridation of silica-coated mesoporous amorphous Ta_2O_5 and successive alkaline treatment enabled the preparation of crystallized mesoporous Ta_3N_5 while retaining the mesoporosity and mesoporous structure of the original Ta_2O_5.

During the nitridation of silica-coated mesoporous Ta_2O_5, the incorporation of N^{3-} ions derived from NH_3 molecules into the Ta_2O_5 framework and the elimination of O^{2-} ions occurs simultaneously through the silica layer deposited on the pore wall surface. Preliminary XPS analysis revealed that the binding energy of the Si 2s orbital was 153.5 eV for the nitridation products, which is significantly lower than those of SiO_2 (154.2 eV) and SiO_x/Si (153.9 eV).[28,29] Because the nitridation of silica occurs at 873 K,[30] the silica layer is thought to be partly nitrided during the thermal nitridation treatment. Partial nitridation of the silica layer led to heterogeneous shrinkage of the silioxane framework and the formation of defects of the silica coating. In addition, our previous

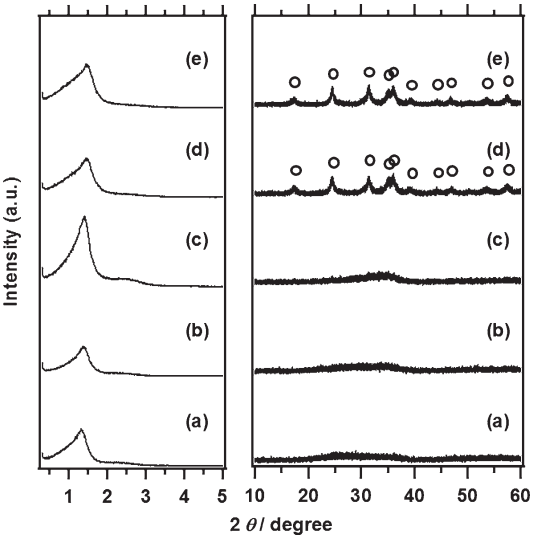

Figure 4. XRD patterns of (a) silica-coated mesoporous Ta_2O_5 and (b−e) nitridation products. Nitridation temperature: (b) 873, (c) 973, (d) 1073, and (e) 1123 K. Nitridation time: 15 h. The diffraction peaks assigned to Ta_3N_5 are marked by open circles.

study suggested that, upon calcination at high temperatures, Ta_2O_5 became partly exposed even in the presence of a silica scaffold, presumably because of condensation of the silica.[9] It is therefore speculated that N^{3-} ions were incorporated into the pore wall through the cracks in the silica layer. As a result, phase transition from Ta_2O_5 to Ta_3N_5 occurred even in the presence of a silica layer on the surface.

3.2. Nitridation Conditions for Preparation of Crystallized Mesoporous Ta_3N_5. Figure 4 shows XRD patterns for silica-coated mesoporous Ta_2O_5 and the products after nitridation at 873−1123 K for 15 h. In the small-angle region, an intense diffraction peak derived from the mesoporous structure was present after nitridation. The peak position gradually shifted from $2\theta = 1.28°$ to $2\theta = 1.49°$ with increasing nitridation temperature as a result of the shrinkage of the mesopore wall and the mesoporous structure during the crystallization/nitridation processes as mentioned in the previous section. In the wide-angle region, no clear diffraction peaks were observed at nitridation temperatures below 973 K, and broad diffraction peaks for the orthorhombic Ta_3N_5 phase emerged at 1073 and 1123 K without any accompanying crystalline impurities such as Ta_2O_5 and TaON. Peak intensity and half-maximum full-width did not show significant changes between the nitridation products at 1073 and 1123 K, indicating that Ta_3N_5 crystallites did not grow. This is because mass transfer was significantly limited in the thin-wall structure reinforced by a silica scaffold.

UV−visible diffuse reflection spectra for the nitridation products at the various temperatures are shown in Figure 5. Amorphous mesoporous Ta_2O_5 did not absorb visible light because its bandgap energy was as large as 3.9 eV, corresponding to 320 nm in terms of absorption edge wavelength. The samples subjected to nitridation above 773 K absorbed visible light ($\lambda > 400$ nm). In general, the valence band top of an (oxy)nitride is located at

(27) Langford, J. I.; Wilson, A. J. C. *J. Appl. Crystallogr.* **1978**, *11*, 102–113.
(28) Anpo, M.; Nakaya, H.; Kodama, S.; Kubokawa, Y.; Domen, K.; Onishi, T. *J. Phys. Chem.* **1986**, *90*, 1633–1636.
(29) Bekkay, Y.; Sacher, E.; Yelon, A. *Surf. Sci.* **1989**, *217*, L377–L381.
(30) Chino, N.; Okubo, T. *Microporous Mesoporous Mater.* **2005**, *87*, 15–22.

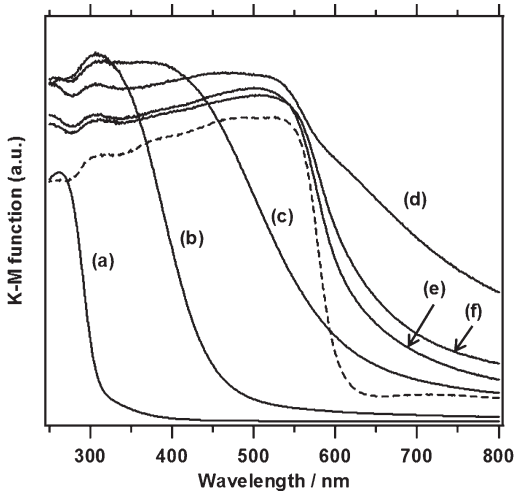

Figure 5. UV−vis diffuse reflection spectra of (a) silica-coated mesoporous Ta_2O_5 and (b−f) the nitridation products. Nitridation temperature: (b) 773, (c) 873, (d) 973, (e) 1073, and (f) 1123 K. Nitridation time: 15 h. The spectrum of bulk Ta_3N_5 is shown by a dashed line for reference.

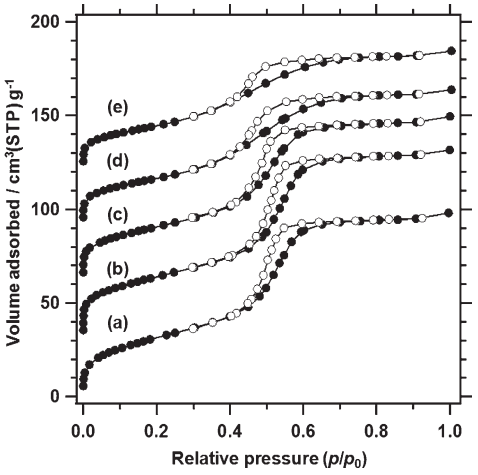

Figure 6. N_2 adsorption−desorption isotherms of (a) silica-coated mesoporous Ta_2O_5 and (b−e) the nitridation products. Nitridation temperature: (b) 873, (c) 973, (d) 1073, and (e) 1123 K. Nitridation time: 15 h. The isotherms are shifted by 30 $cm^3(STP)\ g^{-1}$, respectively.

more negative potential than that of the corresponding oxide because the N 2p orbital, located at a more negative potential than the O 2p orbital, is involved in the formation of the valence band in an (oxy)nitride. As a result, an (oxy)nitride has a narrower band gap than the corresponding oxide. The visible light absorption of the nitrided samples was thus attributable to the incorporation of N^{3-} anions into the crystal structure. The visible light absorption of the samples nitrided below 973 K clearly indicates that a certain portion of the O^{2-} anions was replaced by N^{3-} anions in the mesoporous framework although crystallization into the Ta_3N_5 phase did not occur. The absorption wavelength expanded into the longer wavelength region with increasing nitridation temperature, suggesting that the light absorption wavelength reflected the amount of N^{3-} introduced into the framework. The sample nitrided at 1073 K showed an absorption edge around 600 nm, indicative of the Ta_3N_5 phase in mesoporous solids,[18] which was consistent with the XRD analysis result that crystallization into Ta_3N_5 was achieved at 1073 K. Note that light absorption in the longer wavelength region above 600 nm was prominent for the nitridation product at 973 K. This absorption would be associated with impurity levels. An appreciable degree of N^{3-} anion incorporation seemed to be taking place, while hardly any crystallization occurred in the Ta_3N_5 structure at this temperature, which would produce a significant density of lattice defects in the nitridation product. The broad light absorption observed for the nitridation product at 1123 K was mainly attributed to intraband transition of d electrons from the reduced Ta species that formed as a result of the severe nitridation temperature. In the present case, the broad light absorption would also arise from the partly nitrided silica scaffold, because it was weakened by the alkaline treatment used to remove the silica (see Figure S2 in the Supporting Information).

The N_2 adsorption−desorption isotherms and the BET surface areas and pore volumes of the nitridation products at different temperatures are shown in Figure 6 and Figure S3 in the Supporting Information, respectively. All the isotherms were assignable to a type IV pattern, indicating that the mesoporosity of the original materials was preserved under the present nitridation conditions. BET surface area and pore volume decreased with increasing nitridation temperature. This was because of the inhomogeneous shrinkage of pore wall and the partial degradation of mesoporous structure as nitridation proceeded, which was evident from the visible light absorption of the nitridation products at different temperatures. On the basis of the crystallinity, optical properties, and mesoporosity of the nitridation products, the optimum nitridation temperature for the preparation of crystallized mesoporous Ta_3N_5 was determined to be 1073 K.

Next, the nitridation process from amorphous Ta_2O_5 to crystallized Ta_3N_5 was investigated at the optimum temperature (1073 K) for varying nitridation times. XRD patterns, N_2 adsorption−desorption isotherms, and the BET surface areas and pore volumes of mesoporous Ta_2O_5 and the nitridation products at 1073 K for various nitridation times are shown in Figures 7 and 8 and Figure S4 in the Supporting Information. A diffraction peak at $2\theta = 1.32°$ attributable to the mesoporous structure in the starting Ta_2O_5 shifted to $2\theta = 1.46°$ in 3 h. Diffraction peaks of the orthorhombic Ta_3N_5 phase emerged in samples nitrided for 3 h. No crystalline Ta_2O_5 or TaON phases were detected as intermediate phases in the XRD patterns. Intensities and half-maximum full-widths of the diffraction peaks of Ta_3N_5 samples did not change even for nitridation times of up to 30 h. These observations were in good agreement with the changes in mesoporosity of the samples with increasing nitridation time: although BET surface areas, pore volumes, and pore sizes decreased during the initial 3 h, these properties did not change significantly after the phase transition to orthorhombic Ta_3N_5. Wall thicknesses of the mesoporous Ta_3N_5, roughly estimated to be 3 nm under the assumption of perfect two-dimensional hexagonal ordering of the mesopore channels, also showed good agreement

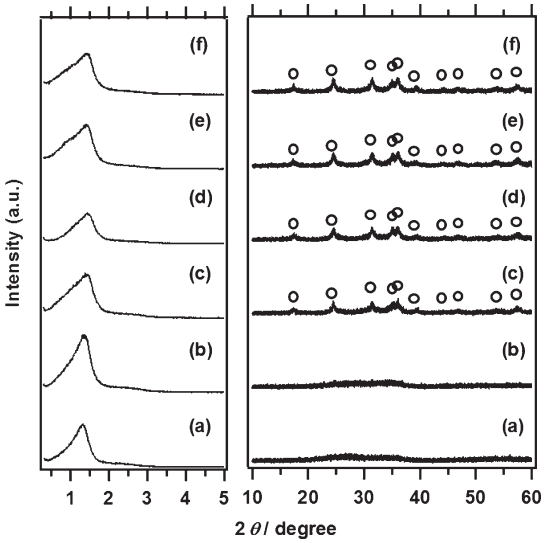

Figure 7. XRD patterns of (a) silica-coated mesoporous Ta_2O_5 and (b−f) the nitridation products. Nitridation time: (b) 0.5, (c) 3, (d) 7, (e) 15, and (f) 30 h. Nitridation temperature: 1073 K. The diffraction peaks assigned to Ta_3N_5 are marked by open circles.

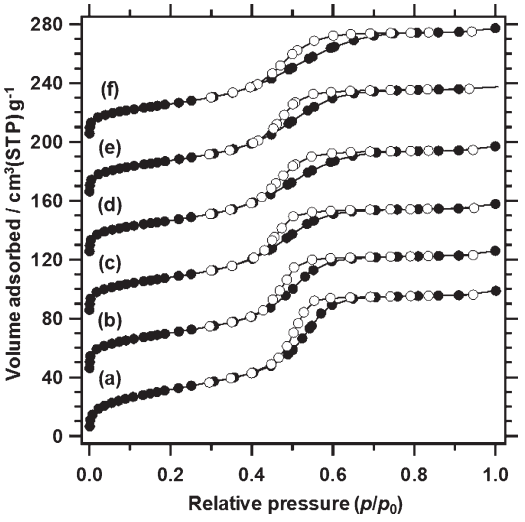

Figure 8. N_2 adsorption−desorption isotherms of (a) silica-coated mesoporous Ta_2O_5 and (b−f) the nitridation products of silica-treated mesoporous Ta_2O_5. Nitridation time: (b) 0.5, (c) 3, (d) 7, (e) 15, and (f) 30 h. Nitridation temperature: 1073 K. The isotherm are shifted by 40 $cm^3(STP)\ g^{-1}$, respectively.

with TEM observations (c.a. 2 nm). UV−visible diffuse reflection spectra for the nitridation products at the various temperatures are shown in Figure S5 in the Supporting Information. Nitridation of the silica-coated Ta_2O_5 precursor for 0.5 h resulted in broad absorption over visible light region (see Figure S5a in the Supporting Information), because of the incorporation of a certain amount of N^{3-} anions into the amorphous Ta_2O_5 framework. The samples nitrided for more than 3 h (see Figure S5b−f in the Supporting Information) have similar light absorption characteristic of Ta_3N_5 reflecting the formation of Ta_3N_5 phase in the resulting materials, although the absorption due to reduced Ta species and partly nitrided silica layers was simultaneously observed.

Thus, crystallization/nitridation of mesoporous Ta_2O_5 into Ta_3N_5 was accomplished by nitridation at 1073 K for 3 h, whereas bulky Ta_3N_5 was prepared by nitridation of Ta_2O_5 at 1123 K for more than 10 h under NH_3 atmosphere. The rapid nitridation into Ta_3N_5 resulted from the thin-wall structure of the Ta_2O_5 precursor, where reconstruction of the constituent elements occurred only in the range of the wall thickness (ca. 2 nm), and thus the nitridation reaction proceeded efficiently, similarly to the case of nanoparticulate Ta_2O_5.[31] Although bulk crystalline Ta_2O_5 could be converted into bulk Ta_3N_5 via the formation of metastable TaON,[32] neither crystalline Ta_2O_5 nor TaON were detected as intermediate phases during the production of crystallized mesoporous Ta_3N_5. This suggests that amorphous mesoporous Ta_2O_5 was directly converted into the orthorhombic Ta_3N_5 phase. It is difficult to obtain metastable TaON by nitriding Ta_2O_5 with NH_3 because of the high reactivity of mesoporous Ta_2O_5 for nitridation and the relatively low thermodynamic stability of the TaON phase.[33]

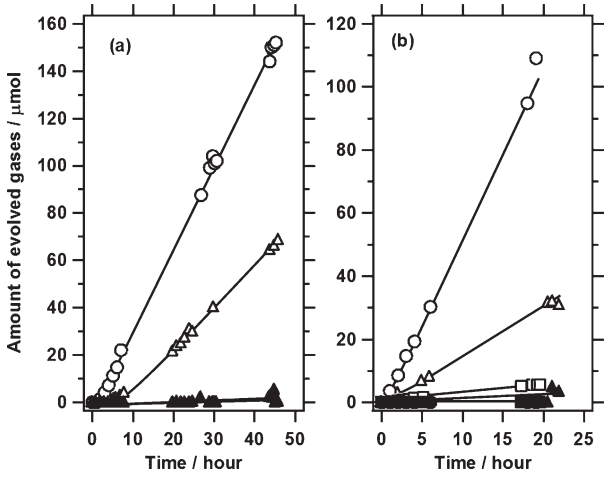

Figure 9. Time dependences of the amount of evolved H_2 from aqueous methanol solution under visible light irradiation ($\lambda > 420$ nm). (a) Reaction using mesoporous Ta_3N_5 with (circles) and without (squares) alkaline treatment. The photocatalysts were loaded with 3 wt % Pt. (b) Reaction using mesoporous Ta_3N_5 after alkaline treatment (circles), conventional bulk Ta_3N_5 (triangles), and standard TiO_2 (triangles). The photocatalysts were loaded with 0.05 wt % Pt. Open and closed symbols indicate H_2 and N_2 evolution, respectively.

3.3. Photocatalytic H_2 Evolution Using Mesoporous Ta_3N_5. Mesoporous Ta_3N_5 loaded with Pt showed photocatalytic activity for the H_2 evolution reaction from an aqueous methanol solution under visible light irradiation. Figure 9a shows time dependences of the amount of evolved H_2 using mesoporous Ta_3N_5 with and without alkaline treatment. The H_2 evolution rate of the mesoporous Ta_3N_5 loaded with 3 wt % Pt increased from 1.8 to 3.4 $\mu mol\ h^{-1}$ after a 4 h alkaline treatment at room temperature. The improvement in photocatalytic activity can be thus attributed to the removal of impurities blocking the active surface sites of the resulting mesoporous Ta_3N_5. Figure 9b shows time dependences of the amount of evolved H_2 using mesoporous and bulk Ta_3N_5,

(31) Zhang, Q.; Gao, L. *Langmuir* **2004**, *20*, 9821–9827.
(32) Takata, T.; Hitoki, G.; Kondo, J. N.; Hara, M.; Kobayashi, H.; Domen, K. *Res. Chem. Intermed.* **2007**, *33*, 13–25.
(33) Orhan, E.; Tessier, F; Marchand, R. *Solid State Sci.* **2002**, *4*, 1071–1076.

and standard TiO_2 modified with 0.05 wt % Pt under visible light irradiation. In the case of mesoporous Ta_3N_5, H_2 evolved steadily during the irradiation for 20 h without notable formation of N_2, indicating that there was negligible oxidation of the nitride framework by photoexcited holes during the irradiation. The H_2 evolution rate of the mesoporous Ta_3N_5 was three times that of conventional bulk Ta_3N_5 under the same reaction conditions although the crystallinity, a vital factor for high photocatalytic activity, was relatively low. The thin-wall structure of the Ta_3N_5 (ca. 2 nm) could reduce the migration distance of photoexcited electrons and holes to surface reactive sites, allowing more photoexcited carriers to induce a photocatalytic reaction. Furthermore, the mesoporous Ta_3N_5 exhibited the H_2 evolution rate 1 order of magnitude higher than the standard TiO_2 under visible light irradiation. The poor activity of TiO_2 was derived from the inadequate ability for visible light absorption. These suggest that mesoporous nitrides have great advantages in the case of photocatalytic reactions under visible-light irradiation. The apparent quantum efficiency of mesoporous Ta_3N_5 under the present reaction condition was estimated to be less than 0.1%, comparable with that of bulk Ta_3N_5[18] although mesoporous Ta_3N_5 was able to evolve H_2 more efficiently than the corresponding bulk Ta_3N_5. This discrepancy may result from differences in loading methods of Pt and reaction conditions. However, it is difficult to estimate the differences in the apparent quantum efficiencies of these materials precisely because of the low efficiency of both mesoporous and bulk Ta_3N_5. In addition, the mesoporous Ta_3N_5 as well as bulk Ta_3N_5 showed no activity for overall water splitting under visible light irradiation. These results suggest that the crystallized thin wall structure of Ta_3N_5 can enhance the photocatalytic activity of H_2 evolution in the presence of sacrificial reagents, but not be applied to overall water splitting at the present stage.

Photocatalytic activity of the mesoporous Ta_3N_5 improved by a factor of 3 even though the BET surface area increased by approximately an order of magnitude. It is worth noting that a loading of 0.05 wt % Pt gave mesoporous Ta_3N_5 a higher H_2 evolution rate than a loading of 3 wt % Pt. TEM observation indicated that aggregated Pt particles were deposited locally on the outer surface of the mesoporous Ta_3N_5 at a relatively low Pt loading rate (0.05 wt %) by the present modification method (see Figure S6 in the Supporting Information). As such, the high specific surface area attributable to the mesoporosity of Ta_3N_5 was not fully utilized. On the contrary, the high Pt loading enhanced the aggregation of Pt particles, preventing migration of photoexcited electrons at grain boundaries between the Pt aggregates. On the other hand, preliminary XPS analysis suggested that the surface of mesoporous Ta_3N_5 was partly hydrolyzed during the alkaline treatment. As a result, amorphous Ta-hydroxides and oxides were formed on the surface as an impurity, although not detected in XRD patterns, diffuse reflection spectra, or N_2 adsorption−desorption isotherms. Such surface impurities in addition to the low crystallinity of thin-wall structure could obstruct charge transfer, enhance charge recombination, and thus deteriorate the photocatalytic activity. Therefore, high dispersion of cocatalysts, high crystallinity of the pore wall, and optimization of silica-removal treatment would enable mesoporous Ta_3N_5 to improve the photocatalytic activity under visible light, and the resulting Ta_3N_5 would be applicable to Z-scheme type reaction in which photocatalysts that have not attained overall water splitting can be employed.[19,20]

4. Conclusions

Ta_3N_5 with a crystalline mesoporous framework and a high specific surface area was obtained through nitridation of silica-coated mesoporous Ta_2O_5 with amorphous framework under NH_3 flow. The silica layer deposited by the CVD treatment of TMOS functioned effectively as a scaffold against phase transformation, preserving the original mesoporosity during the crystallization and nitridation of mesoporous Ta_2O_5. Direct phase transition from amorphous Ta_2O_5 to orthorhombic Ta_3N_5 was achieved by the nitridation of silica-coated mesoporous Ta_2O_5 at 1073 K for 3 h under NH_3 flow. The original arrangement of the pore channels was slightly distorted in crystallized mesoporous Ta_3N_5 because crystallization in the Ta_3N_5 phase was accompanied by shrinkage of the mesopore wall, which resulted from the substitution of 2 N^{3-} anions for 3 O^{2-} anions during nitridation. However, after the crystallization into Ta_3N_5, the porous structure was not affected significantly by prolonged nitridation at 1073 K.

The crystallized mesoporous Ta_3N_5 modified with Pt exhibited photocatalytic activity for the H_2 evolution reaction from an aqueous methanol solution under visible light irradiation. The photocatalytic performance of crystallized mesoporous Ta_3N_5 was superior to that of conventional bulk Ta_3N_5, because of the former's thin-wall structure (~2 nm in thickness), which promotes charge transfer to active surface sites. These results validated the effectiveness of crystalline mesoporous nitrides, which enable efficient charge transfer to surface active sites in response to visible light, in photocatalytic applications.

Acknowledgment. This work was supported by the Solution Oriented Research for Science and Technology (SORST) program of the Japan Science and Technology (JST) Agency and the 21st Century Center of Excellence (COE) program of the Ministry of Education, Culture, Sports, Science and Technology of Japan.

Supporting Information Available: Pore size distribution curves of mesoporous Ta_2O_5 and Ta_3N_5; diffuse reflection spectra; BET surface areas and pore volumes of mesoporous Ta_3N_5; and a TEM image of mesoporous Ta_3N_5 loaded with 0.05 wt % Pt by in situ photodeposition. This material is available free of charge via the Internet at http://pubs.acs.org.